Stability, structure, and electronic properties of chemisorbed oxygen and thin surface oxides on Ir(111)

Hong Zhang,[1,2] Aloysius Soon,[1,*] Bernard Delley,[3] and Catherine Stampfl[1]
[1]*School of Physics, The University of Sydney, Sydney NSW 2006, Australia*
[2]*School of Physical Science and Technology, Sichuan University, Chengdu 610065, People's Republic of China*
[3]*Paul Scherrer Institut, WHGA/123, CH-5232, Villigen PSI, Switzerland*
(Received 18 February 2008; revised manuscript received 10 June 2008; published 31 July 2008)

We present *ab initio* calculations for atomic oxygen adsorption on Ir(111) for a wide range of oxygen coverages, Θ, namely from 0.11 to 2.0 monolayers (ML), including subsurface adsorption and thin surface-oxide-like structures. For on-surface adsorption, oxygen prefers the fcc-hollow site for all coverages considered. Similarly to oxygen adsorption on other transition metal surfaces, as Θ increases from 0.25 ML to 1.0 ML, the binding energy decreases, indicating a repulsive interaction between the adsorbates. For the coverage range of 0.11 to 0.25 ML, there is an attractive interaction, suggesting the possible formation of a local (2×2) periodicity with a local coverage of $\Theta=0.25$ ML. Pure subsurface oxygen adsorption is found to be metastable and endothermic with respect to the free O_2 molecule. For structures with coverage beyond one full ML, we find the incorporation of oxygen under the first Ir layer to be exothermic. As the subsurface O coverage increases in these structures from 0.5 to 1.0 ML, the energy becomes slightly more favorable, indicating an attractive interaction between the O atoms. The structure with the strongest average O binding energy is however a reconstructed trilayer-like structure that can be described as a $(\sqrt{3}\times\sqrt{3})R30°$ oxide-like layer in $p(2\times2)$ surface unit cell, with coverage 1.5 ML. Through calculation of the surface Gibbs free energy of adsorption, taking into account the pressure and temperature dependence through the oxygen atom chemical potential, the calculations predict only three thermodynamically stable regions, namely, the clean surface, the $p(2\times2)$-O phase, and bulk IrO_2. Thin trilayer surface oxide structures are predicted only to form when kinetic hindering occurs, in agreement with recent experimental work.

DOI: 10.1103/PhysRevB.78.045436 PACS number(s): 81.65.Mq, 68.43.−h, 68.47.Gh

I. INTRODUCTION

Obtaining a detailed knowledge of the surface structure and stoichiometry is crucial for understanding the physical and chemical properties of advanced materials such as those used in heterogeneous catalysis, corrosion resistance, electronic devices, sensors, and fuel cells.[1–3] This knowledge is also central for enhancing the performance of existing catalysts as well as developing new ones.[4] Many current industrial processes involve catalytic oxidation reactions,[5] where the catalysts are typically transition metal particles dispersed on oxide supports.[6] The importance of transition metals (TMs) for such reactions has motivated large numbers of studies on oxygen-metal interactions at low index surfaces of TMs with the aim of obtaining a better understanding of the underlying mechanisms.[7–9] For example, oxygen adsorption on Ru(0001),[10–14] Rh(111),[15,16] Pd(111),[17,18] Ag(111),[19–24] Ni(111),[25] Cu(111),[5] Pt(111)[26,27], and Au(111)[28] surfaces has been studied in detail theoretically. Recently, a trend study addressing the incorporation of oxygen into the basal plane of the late 4*d* TMs from Ru, Rh, Pd to Ag was carried out.[29] It was found that occupation of subsurface sites is connected with a significant distortion of the host lattice, rendering it initially less favorable than on-surface chemisorption. Oxygen penetration below the surface of the substrate only starts after a critical coverage, and is a key signature for oxide formation at transition metal surfaces. The initial coverage was found to be lower for the TMs to the right in the Periodic Table, which bind O more weakly.

On the experimental side, many techniques such as AES (Auger electron spectroscopy), EELS (electron-energy-loss spectroscopy), HREELS (high-resolution electron-energy-loss spectroscopy), LEED (low-energy electron diffraction), NEXAFS (near-edge x-ray-absorption fine structure), STM (scanning tunneling microscopy), TDS (thermal desorption spectroscopy), TPD (temperature programmed desorption), and XPS (x-ray photoelectron spectroscopy) have been applied to help determine the structure of surfaces.[30,31] One or several of these techniques have been used to study oxygen adsorption on Ru(0001),[32] Rh(111),[33] Pd(111),[34,35] Ni(111),[36,37] Cu(111),[38,39] Pt(111)[40], and Au(111).[41]

As a late 5*d* transition metal, iridium shows potential in a great variety of applications, particularly as a heterogeneous catalyst in various industrial chemical reactions:[42] Ir and Ir-alloy catalysts are widely used in reactions that require the activation of strong C-H bonds. It has been shown that oxygen-precovered Ir(111) catalyzes the oxidization of propylene and isobutylene to produce acetone.[43] These olefins are cleaved at the C=C double bond on the iridium surface to form ketones and carboxylic acids,[44] producing no side products which are often seen when other catalysts are used. An example of such organic reaction catalysis is the use of Ir-based catalysts to improve the production of acetic acid by a methanol carbonylation process.[45] With the increased demand for clean alternative energy, iridium is also now seen as a potential catalyst for CO_x-free production of hydrogen from ammonia[46] and gasoline[47] to be used as fuel in automobile fuel cells. In addition, it is also considered as an improvement to the automobile catalytic converter because of its unique ability to decompose NO as well as reduce NO_x in the presence of hydrocarbons.[48] Clearly, a more detailed

atomic-level understanding of the interactions of these gas phase species with Ir surfaces would be very valuable, which could lead to improved Ir-based catalysts with greater selectivity and activity.

Since the interaction of the iridium catalyst with an oxidizing environment is common to several important heterogeneous reactions mentioned above, we address this in the present paper using first-principles calculations. We focus on the (111) surface and present results for oxygen adsorption and initial oxidation, and determine the pressure-temperature phase diagram for conditions extending from ultrahigh vacuum to those typical of technical catalysis, comparing the results to other O/TM systems. The interaction of atomic oxygen with single crystal Ir(111) surfaces has been the subject of several experimental studies. LEED (Ref. 49) and ultraviolet photoelectron spectroscopy (UPS) studies showed that exposure of a clean Ir(111) surface to oxygen produces a (2×2) LEED pattern.[50] Such a pattern could either be caused by a $p(2\times2)$ surface structure or by three domains of a (1×2) surface structure rotated by 120° with respect to one another. The (1×2) surface structure corresponds to a coverage of 1/2 ML. XPS and HREELS (Refs. 51 and 52) studies found that 1/2 ML was the maximum coverage for atomic oxygen. A single chemisorbed state for atomic oxygen on Ir(111) was perceived from the observation of a single loss peak in EELS spectra at 550 cm^{-1} at the saturation coverage.[53]

With regard to theoretical investigations, chemisorption of atomic O on Ir(111) was studied by using first-principles density functional theory (DFT) calculations.[54,55] The preferred binding site, atomic structure and vibrational frequencies at 0.25 ML coverage, calculated in a $p(2\times2)$ surface unit cell, were reported. It was found that atomic oxygen adsorbs preferentially in the threefold fcc-hollow site. *Ab initio* investigations of oxygen adsorption on Ir(111) have therefore been limited to a very narrow range of oxygen coverage, and to zero pressure and zero temperature. Often the results obtained in such studies cannot be extrapolated directly to the technologically relevant situation of finite temperature and high pressure.[2] In particular, possible oxidation of the surface in a reactive oxygen-rich environment has been thought to lead to the formation of an inactive surface oxide outer layer, poisoning the catalytic reaction. However, conversely it could well play the role of the active centers, as seen in other O/TM systems.[56] Upon exposure to an oxygen atmosphere, the structures formed on the surfaces may vary from simple adlayers of chemisorbed oxygen, to oxygen diffusion into the subsurface region and the formation of oxides, depending on the partial pressure, temperature, and orientation of the metal substrate. Oxidation catalysts can be rather complex, often involving multiple phases and various active sites. Hence a careful study of the role of each phase and its specific interaction under working conditions is required to suggest efficient ways of catalyst improvement.

II. CALCULATION METHOD

All calculations are performed using DFT as implemented in the all-electron $DMol^3$ code,[57,58] where we employ the generalized gradient approximation (GGA) of Perdew, Burke, Ernzerhof (PBE) for the exchange-correlation functional.[59] The Ir(111) surface is modeled using a supercell approach, where we use seven-layer Ir(111) slabs with a vacuum region of 25 Å. Oxygen atoms are adsorbed on both sides of the slab, preserving inversion symmetry. The oxygen atoms and the outmost two Ir layers are allowed to fully relax. To obtain highly converged surface properties, it is necessary that bulk and surface calculations are performed with the same high accuracy.[60] The wave functions are expanded in terms of a double-numerical quality localized basis set with a real-space cutoff of 10 bohr for both the bulk and the surface. Polarization functions and scalar-relativistic corrections are also incorporated explicitly. We consider oxygen coverages from 0.11 ML to 2.00 ML using (3×3), (2×2), and (1×1) surface unit cells in which adsorption in various on-surface and subsurface sites, as well as surface-oxide-like structures, were investigated as explained below. The total energy, force on the atoms, and displacements are converged to within 1×10^{-6} Ha(2.7×10^{-5} eV), 3×10^{-4} Ha/Bohr(1.5×10^{-2} eV/Å), and 3×10^{-4} Bohr(1.6×10^{-2} Å), respectively, in the DFT self-consistent cycles. The Brillouin-zone integrations are performed using a $(12\times12\times1)$ Monkhorst-Pack (MP) grid for the (1×1) surface unit cell, yielding 19 special **k**-points in the irreducible part of the surface Brillouin zone. We find that the change in cohesive energy of bulk Ir is less than 10 meV per Ir atom when increasing the real-space cutoff radius from 8 to 12 bohr. To test the variation of the change in cohesive energy of bulk Ir as a function of the **k**-point mesh density, we vary the MP integration grids, denoted by $(M\times M\times M)$, with M taking (even) values of 6 to 16. The variation is found to be less than 3 meV per Ir atom when changing the **k**-point mesh from $M=10$ to 16. Thus, for bulk Ir calculations, we adopt a cut-off radius of 10 bohr and a MP **k**-point mesh of $(12\times12\times12)$. Using the same cut-off radius for the slab calculations, we also find that increasing the **k**-mesh for the surface unit cell from $(6\times6\times1)$ to $(16\times16\times1)$ changes the surface energy of Ir(111) by 3 meV/$Å^2$. For the surface calculations, we use a MP **k**-point mesh of $(12\times12\times1)$ for the surface unit cell, and this **k**-point mesh is folded accordingly for larger surface cells.

We address the stability of O/Ir(111) structures with respect to adsorption of O by calculating the average binding energy per O adatom. The average binding energy per oxygen atom, $E_b^{O/Ir}$, is defined as

$$E_b^{O/Ir} = -1/N_O[E^{O/Ir} - (E^{Ir} + N_O E^O)], \quad (1)$$

where N_O, $E^{O/Ir}$, E^{Ir}, and E^O, are the number of oxygen atoms in the surface unit cell, the total energies of the adsorbate-substrate system, the clean surface, and the free oxygen atom, respectively. The binding energy is the energy that a free oxygen atom gains upon adsorption on the Ir surface. For the formation of a surface oxide, the average adsorption energy is defined as

$$E_{ad}^{surf.\text{-}oxide} = -1/N_O[E^{O/Ir} - (E^{Ir} + N_O E^O + \Delta N_{Ir} E_{Ir}^{bulk})], \quad (2)$$

where ΔN_{Ir} is defined to be the difference in the number of Ir atoms of the surface structure compared to the ideal Ir(111)

substrate layer, and $E_{\mathrm{Ir}}^{\mathrm{bulk}}$ is the total energy of an iridium atom in bulk. This term appears since the missing Ir atoms are assumed to be rebound at kink sites at steps, which contribute an energy equal to that of a bulk Ir atom. To analyze the nature of bonding, we consider the difference electron density,

$$n^{\Delta}(\mathbf{r}) = n(\mathbf{r}) - n^{0}(\mathbf{r}) - n^{\mathrm{O}}(\mathbf{r}), \tag{3}$$

where $n(\mathbf{r})$ is the total electron density of the adsorbate-substrate system, and $n^{0}(\mathbf{r})$ and $n^{\mathrm{O}}(\mathbf{r})$ are the electron densities of the clean substrate and the free oxygen atom, respectively, where the atomic geometry of the substrate is that of the relaxed adsorbate system (but without the O atoms). This quantity then shows from which regions the electron density has been depleted and increased due to O adsorption on the surface.

Using the Helmholtz equation, the surface dipole moment (in Debye) is calculated according to the formula

$$\mu = \frac{A\Delta\Phi}{12\pi\Theta}, \tag{4}$$

where A is the surface area in Å^2 per (1×1) surface unit cell, and $\Delta\Phi$ is the work-function change in eV. In order to investigate the effect of pressure and temperature on the stability of the various structures, we calculate the surface free energy of adsorption,

$$\gamma(T,p) = (\Delta G - \Delta N_{\mathrm{Ir}}\mu_{\mathrm{Ir}} - N_{\mathrm{O}}\mu_{\mathrm{O}})/A, \tag{5}$$

where $\Delta G = G_{\mathrm{O/Ir(111)}}^{\mathrm{slab}} - G_{\mathrm{Ir(111)}}^{\mathrm{slab}}$, and the first and second terms on the right-hand side are the free energies of the O/Ir surface under consideration and the clean Ir(111) slab, respectively. μ_{O} and μ_{Ir} are the O and Ir atom chemical potentials, which for μ_{Ir} is the free energy of an Ir atom in bulk fcc iridium. The temperature (T) and pressure (p) dependences enter mainly through the oxygen chemical potential, μ_{O},[61]

$$\mu_{\mathrm{O}}(T,p) = 1/2\left[E_{\mathrm{O}_2}^{\mathrm{total}} + \tilde{\mu}_{\mathrm{O}_2}(T,p^0) + k_B T \ln\left(\frac{p_{\mathrm{O}_2}}{p^0}\right)\right], \tag{6}$$

where p^0 corresponds to atmospheric pressure and $\tilde{\mu}_{\mathrm{O}_2}(T,p^0)$ includes the contribution from rotations and vibrations of the molecule, as well as the ideal-gas entropy at 1 atmosphere.[61] $E_{\mathrm{O}_2}^{\mathrm{total}}$ is the total energy of the oxygen molecule. For $\tilde{\mu}_{\mathrm{O}_2}(T,p^0)$ we use the experimental values from thermodynamic tables.[62]

When calculating the difference $\Delta G = G_{\mathrm{O/Ir(111)}}^{\mathrm{slab}} - G_{\mathrm{Ir(111)}}^{\mathrm{slab}}$, one needs to calculate the Gibbs free energies of both the adsorption and reference systems. Recent studies (e.g., Ref. 63) have shown that for O/TM systems a good approximation is to use the total energies from the DFT calculations which is what we have done in the present work. The relationship between the total energies of DFT calculations and the Gibbs free energies of the systems has been discussed in detail in the literature.[61] Briefly, the contributions due to the vibrational free energy, configurational entropy and the pressure-volume (pV) term are present in the Gibbs free energies. The pV term is of the order of tenths of meV/Å^2, from a dimensional analysis for the (p,T) ranges we are interested in, and hence can be safely neglected. The vibrational contribution is usually small for such systems, typically less than 10 meV/Å^2 (see Appendix for details). The contribution from configurational entropy is known to be non-negligible at phase transition boundaries,[64] but it is omitted for this study since we only focus on the relative stability of the various structures.

TABLE I. Properties of bulk Ir and the Ir(111) surface and comparison with other *ab initio* calculations and with experiment. a_0 is the lattice constant (in Å), B_0 is the bulk modulus (in Mbar), E_{coh} is the cohesive energy (in eV), and Φ is the work function (in eV).

	Present work	Other *ab initio* calculations	Experimental results
a_0	3.85	3.86[a] (PW91) 3.89[c] (GGA)	3.84[b]
B_0	3.57		3.55[b]
E_{coh}	7.45	7.46[c]	6.94[b]
Φ	5.88	6.63[d]	5.76[e]

[a]Reference 65, calculated using DFT-GGA and the plane-wave pseudopotential approach.
[b]Reference 66.
[c]Reference 67, calculated using DFT-GGA and the plane-wave pseudopotential approach.
[d]Reference 68, calculated using the tight-binding linear-muffin-tin-orbital Green's function technique.
[e]Reference 69.

III. RESULTS

A. Clean Ir(111), bulk Ir and the oxygen molecule

We first consider the properties of bulk Ir and the Ir(111) surface. The calculated properties are listed in Table I (the free Ir atom is calculated including spin polarization). The calculated bulk lattice constant is a_0=3.85 Å neglecting zero-point vibrations. The cohesive energy, E_{coh}, is calculated to be 7.45 eV and the bulk modulus, B_0=3.57 Mbar. The corresponding experimental values are 3.84 Å, 6.94 eV, and 3.55 Mbar.[67] Our values are also in line with other reported DFT-GGA results of a_0=3.89 Å and E_{coh}=7.46 eV.[67] The obtained interlayer relaxations $d_{i,j}$ between layers i and j with respect to the bulk spacing (d =2.224 Å) are $\Delta_{12}=-1.57\%$ and $\Delta_{23}=-0.49\%$ for the topmost layers.[70] To the best of our knowledge, there are no recent experimental results for the surface relaxation of the Ir(111) surface, except the early report of a contraction of $2.5\pm5\%$ for the first interlayer spacing.[71] We can compare our results with that of Rh, the upper neighbor of Ir in the Periodic Table. The contractions of the topmost two interlayer spacings of Ir(111) are slightly smaller than those of the Rh(111) surface obtained from DFT-GGA calculations as implemented in the all-electron full-potential-linearized augmented plane-wave method (FP-LAPW),[71] which are $\Delta_{12}=-1.8\%$ and $\Delta_{23}=-0.9\%$, though the trend is the same. For Rh, the experimental results determined by recent LEED analyses are $\Delta_{12}=-1.4\pm0.9\%$ and $\Delta_{23}=-1.4\pm1.8\%$.[72] For Pt, the right neighbor of Ir, the change in the uppermost two

interlayer spacings are $\Delta_{12}=1.20\%$ and $\Delta_{23}=-0.50\%$, as reported from DFT-GGA calculations using the FP-LAPW method,[60] while the experimental result for Δ_{12} is $1.0\pm0.1\%$.[73] The calculated work function for the clean surface of Ir(111) is 5.88 eV and is in line with the reported experimental value 5.76 eV.[74]

For the oxygen atom and molecule, spin-unrestricted calculations using nonspherical densities are performed where the real-space cutoff for the calculation of both the oxygen atom and oxygen molecule is increased to 20 bohr, the largest basis set available in the DMol^3 code. The binding energy of O_2 is calculated to be 3.04 eV/O atom, while the bond length and vibrational frequency are 1.22 Å and 1527 cm^{-1}, respectively, in excellent agreement with other theoretical results.[58,75,76] The corresponding experimental values[77] are 2.56 eV/atom, 1.21 Å and 1580 cm^{-1}. The typical overestimation of DFT-GGA is observed in the binding energy. The values presented here are indicative of well-converged DFT-GGA calculations, and since our interest lies mainly in the relative stability of various structures, this overbinding will not affect the qualitative conclusions in this paper.

B. On-surface, subsurface, and thin surface-oxide-like structures of oxygen on Ir(111)

For on-surface oxygen adsorption, we calculate the binding energies for a range of coverages Θ: (3×3)-O(Θ=0.11 ML), (2×2)-O(Θ=0.25 ML), (2×2)-2O(Θ=0.50 ML), (2×2)-3O(Θ=0.75 ML), and (2×2)-4O(Θ=1.00 ML). We consider adsorption in the fcc- and hcp-hollow sites, and top sites. For subsurface sites, we calculate adsorption in (i) the octahedral site, denoted hereafter as "octa," and (ii) the tetrahedral sites. There are two types of tetrahedral sites; one is where there are three Ir atoms above it and one below, denoted as tetra-I, and the alternative one, tetra-II, is just the opposite with one surface Ir atom directly above and three below it in the second Ir layer. For 0.25 ML coverage, we also consider the bridge site. For structures involving both on-surface and subsurface O atoms, we start from the (2×2)-4O on-surface configuration and add subsurface oxygen atoms below the surface Ir layer. We investigated three possible site configurations: fcc/tetra-I, fcc/tetra-II, and hcp/octa for various coverages. We performed calculations for oxygen in these different sites up to a total coverage 2.0 ML (see Fig. 1).

Previous studies for O/Rh[15] and O/Ru[10] identified a reconstructed surface-oxide-like structure that is energetically more favorable than the homogeneous chemisorbed phases discussed above. In particular, for Θ=1.50 ML, the atomic configuration of this surface oxide is similar to that of the 2.0 ML "mixed" on-/subsurface structure, except that the O-M-O trilayer (where M=Rh or Ru) is laterally expanded and rotated 30° relative to the underlying substrate such that it consists of three metal atoms and six oxygen atoms in the $p(2\times2)$ cell [instead of four metal and eight oxygen atoms as for in the 2.0 ML "mixed" on-surface+subsurface structure (Fig. 1(d))]. The metal atoms are located in high-symmetry sites, namely, fcc, hcp, and on-top sites. The stoichiometry of this surface oxid-like layer is 1Ir:2O, the same as that of bulk iridium dioxide, IrO_2. This surface structure can be described as a $(\sqrt{3}\times\sqrt{3})R30°$ oxide layer on a $p(2\times2)$/Ir(111) surface unit cell (see Fig. 2, labeled as "$p2$:IrO_2" and referred to "$(3/\sqrt{2}\times\sqrt{2})$" hereafter). The average oxygen binding energy of this structure is 3.94 eV, and it is energetically more favorable than the on-surface O/Ir(111) structure at 1.0 ML oxygen coverage (which has an average binding energy of 3.83 eV). From Fig. 2, it can be seen that the coupling of this O-Ir-O trilayer to the underlying metal is via the lower O. The first Ir(111) interlayer distance, d_{12}, is notably expanded to 3.01 Å which is about 35% larger compared to the Ir bulk value.

We also consider a similar structure, where the O-Ir-O trilayer is laterally shifted such that the lower lying oxygen atoms occupy the above-mentioned high-symmetry sites (instead of the Ir atoms). It is labeled as "$p2$:IrO_2-SR." The average binding energy of oxygen in this structure is calculated to be 3.78 eV.

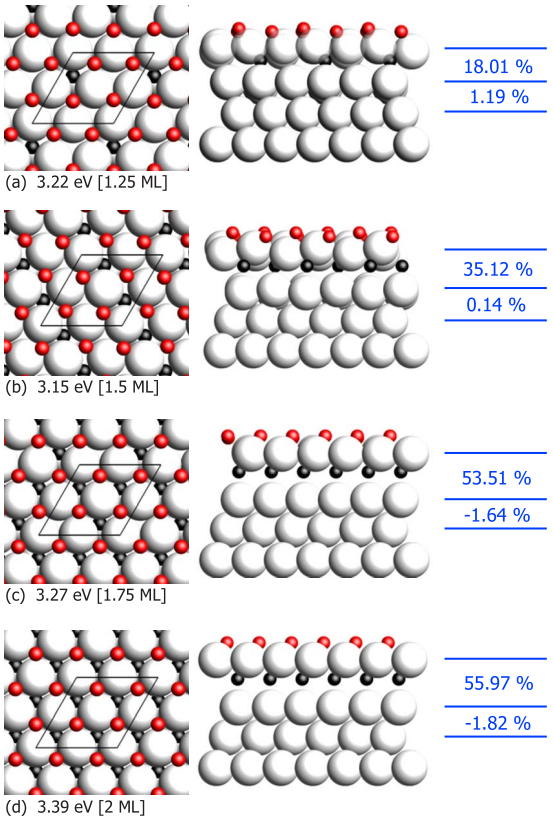

FIG. 1. (Color online) Atomic geometry of oxygen structures with a full monolayer of oxygen on the surface in the fcc site, for increasing subsurface oxygen concentrations, as calculated using a (2×2) surface unit cell. (a) Full monolayer (four oxygen atoms per cell) plus one subsurface oxygen atom in the tetra-I site, (b) as for (a) but with two oxygen atoms in the tetra-I site, (c) and (d) as for (b) but with three and four oxygen atoms in the tetra-I sites, respectively. The average adsorption energy with respect to the clean Ir(111) substrate and free oxygen atoms, as well as the corresponding coverage, are given at the bottom of each figure. The relative variation of the atomic interlayer spacings, with respect to the bulk value, is also given to the right of the figures. The large (gray) and small (red) spheres represent iridium and oxygen atoms, respectively.

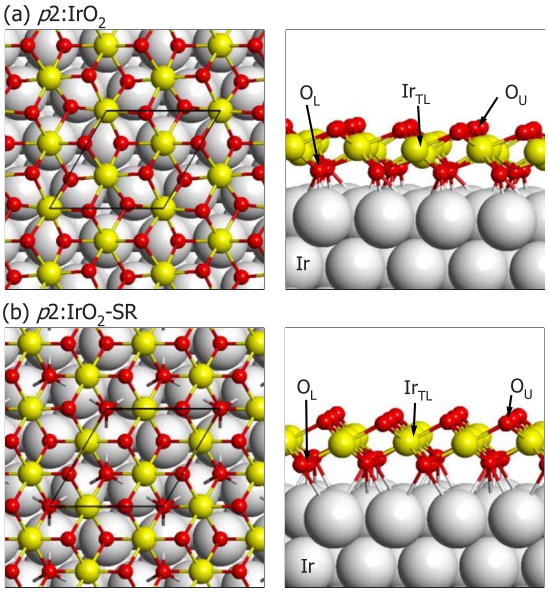

FIG. 2. (Color online) (a) The lowest energy surface-oxide-like structure considered can be described as a reconstructed $(\sqrt{3}\times\sqrt{3})R30°$ surface-oxide-like trilayer in a $p(2\times2)$ surface unit cell. (b) The next most favorable structure, which is the same as (a) except that the upper O-Ir-O trilayer is laterally shifted compared to (a). Oxygen atoms are shown as small dark (red) spheres, while the small gray (yellow) spheres (labeled Ir_{TL}) are the uppermost Iridium atoms (in the trilayer). The large gray spheres are the second and third layer (unreconstructed) iridium atoms. O_U and O_L denote the upper and lower O atoms, respectively.

C. Energetics

The binding energies, E_b, of on-surface oxygen on the Ir(111) surface in the fcc, hcp, on-top, bridge, octa, tetra-I and tetra-II sites, at coverage 0.25 ML are listed in Table II given with respect to the free oxygen atom. In Fig. 3, the average binding energies for the various oxygen structures are plotted as a function of coverage.

It can be seen from Table II that the fcc-hollow site is energetically most favorable. This is in agreement with the experiment LEED study for the (2×2) superstructure.[49] The fcc preference for adsorbed oxygen has been observed on the (111) faces of several other fcc transition metals.[52] Of the subsurface sites considered, the tetra-I site is most favorable. It is, however, significantly less stable than on-surface chemisorption, presumably because of the additional energy cost of distorting the substrate lattice and breaking metal-metal bonds.

TABLE II. The binding energy of oxygen, relative to a free O atom, on Ir(111) for various adsorption sites for 0.25 ML coverage, and comparison with other *ab initio* calculations. The unit of energy is eV.

Site	Present work	Other *ab initio*[a] (PW91, RPBE)
fcc	4.62	4.57,4.00
hcp	4.42	4.32,3.75
Bridge	3.97	4.02,3.51
Top	3.54	3.46,3.04
Octa	−0.38	
Tetra-I	0.78	
Tetra-II	0.52	

[a]Reference 54, DFT-GGA calculations using the pseudopotential plane-wave method.

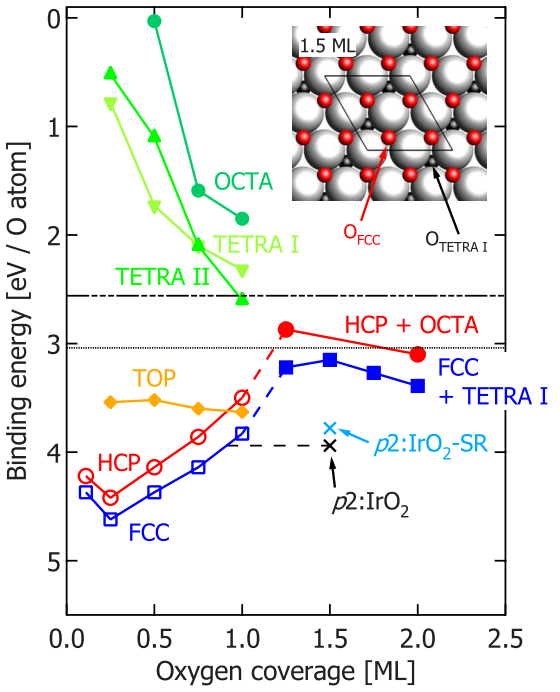

FIG. 3. (Color online) Average binding energy of oxygen on Ir(111) in the on-surface and subsurface sites for various coverages, with respect to the energy of a free oxygen atom. The horizontal upper and lower lines are half the experimental and theoretical binding energies of O_2, respectively. The inset shows the top view of the atomic structure of the (2×2)-$4O_{fcc}/O_{tetra\text{-}I}$ structure containing four oxygen atoms in fcc sites and one oxygen atom in the subsurface tetra-I site (with total coverage 1.25 ML). The large (yellow) and small (red) spheres represent iridium and oxygen atoms, respectively.

From Fig. 3, it can be seen that the binding energy for O on Ir(111) increases modestly in the coverage range from $\Theta=0.11$ to 0.25 ML, and then decreases with oxygen coverage for both the fcc and hcp sites up to $\Theta=1.00$ ML. For oxygen adsorbed in the on-top site, the binding energy varies little with the coverage, with an average value of 3.57 eV. For oxygen in the subsurface octa, tetra-I and tetra-II sites, the binding energy increases rapidly with the oxygen coverage, indicating an effective attractive interaction between O atoms. For the "mixed" on-surface+subsurface structures, it can be seen that they are less favorable than the on-surface configurations, but with increasing coverage they exhibit a slight increase in the binding energy, indicating a weak effective attractive interaction. This increase in average binding energy for increasing coverage (from 0.50 to 1.0 ML) of subsurface oxygen is similar to what has been found for other transition metals (e.g., Rh and Ru). The most energetically favorable of all are the surface-oxide-like structures

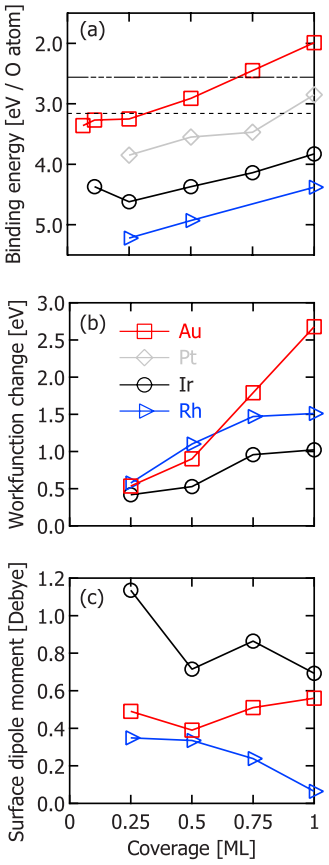

FIG. 4. (Color online) Binding energy (a) of oxygen on the Ir(111), Pt(111) (Ref. 27), Au(111) (Ref. 28), and Rh(111) (Ref. 15) surfaces in the fcc-hollow site for various oxygen coverages. The horizontal upper and lower lines are half the experimental and theoretical binding energies of O_2, respectively. (b) The corresponding work-function change and (c) surface dipole moment for oxygen on Ir(111), Au(111) (Ref. 28), and Rh(111) (Ref. 15).

consisting of an O-Ir-O trilayer with a $(\sqrt{3}\times\sqrt{3})R30°$ periodicity in a (2×2) surface unit cell (shown in Fig. 2). For the most favorable structure, it has an average binding energy slightly more favorable than the full monolayer on-surface structure. As indicated by the dashed line in Fig. 3, for increasing coverages of oxygen, the results indicate that there will be a phase transition from on-surface adsorption to the reconstructed surface-oxide-like structure with local coverage of 1.5 ML.

It is interesting to compare these results with those for O adsorption on Rh(111),[71,78] Ir's upper neighbor in the Periodic Table, and neighbors to the right of it in the Periodic Table, Pt(111) and Au(111). In Fig. 4, we have plotted the binding energies of these systems, where oxygen occupies the fcc sites. It can be seen that the binding energy of oxygen on Rh(111) is stronger than that of Ir(111), e.g., at coverage =0.25 ML it is about 0.60 eV larger. The less exothermic binding energy of O on Ir(111) compared with Rh can be expected from the comparison of the experimental enthalpy of formation of bulk IrO_2 per oxygen atom (−1.42 eV) and that of Rh_2O_3 (−1.78 eV).[79] According to the "Tanaka-Tamaru rule," the initial enthalpies of chemisorption of oxygen and other molecules are linearly related to the enthalpies of formation of the most stable oxides.[80]

The binding energies shown in Fig. 4 decrease progressively for the elements to the right in the Periodic Table, i.e., for Pt and Au, which is due to the continued filling of the *d* band in the late TMs, leading to an increased occupation of antibonding oxygen-metal states.[81] At 0.25 ML, the binding energy is about 0.8 eV less for O/Pt(111) compared to O/Ir(111). The more exothermic binding energy of O on Ir(111) when compared to O/Pt(111) and O/Au(111) is also consistent with the enthalpy of formation of the bulk oxide: For bulk IrO_2, per oxygen atom, it is −1.42 eV (Ref. 79) (theoretical value −1.45 eV) while the experimental enthalpy of formation of PtO_2 is −0.69 eV,[79] and for Au_2O_3 it is −0.135 eV.[82,83]

D. Atomic structure

The calculated atomic geometries of the O/Ir(111) structures (for $\Theta=0.11$ to 1 ML) are listed in Table III, where the binding energy is also included. The relaxed interlayer distances d_{12} and d_{23} for the clean Ir(111) surface are 2.19 Å and 2.21 Å respectively, and the interlayer distance for bulk Ir is 2.22 Å. On adsorption of oxygen at the low coverage of 0.11 ML, the interlayer distances d_{12} and d_{23} are both 2.21 Å showing an expansion of 1.57% for d_{12} relative to the (relaxed) clean surface, and no change for the second interlayer distance. Increasing the oxygen coverage to 0.25 ML, the interlayer distances d_{12} and d_{23} are 2.23 Å and 2.21 Å, re-

TABLE III. Calculated structural parameters (in Å) for various coverages of O in the fcc-hollow site on Ir(111). $d_{Ir/O}$ is the bond length between oxygen and the first-nearest-neighbor iridium atom, d_{01} is the vertical height of oxygen above the topmost iridium layer, and d_{12} and d_{23} are the first and second metal interlayer spacings, respectively, where the center of mass of the layer is used. The calculated interlayer distance for bulk iridium is 2.22 Å. $E_b^{O/Ir}$ is the binding energy in eV with respect to atomic oxygen.

Coverage	0.11	0.25		0.50	0.75	1.00
$d_{O/Ir}$	2.07	2.06	2.04[a]	2.03	2.04	2.02
d_{01}	1.33	1.30	1.22[a]	1.29	1.28	1.27
d_{12}	2.21	2.23		2.25	2.26	2.25
d_{23}	2.21	2.21		2.22	2.22	2.23
$E_b^{O/Ir}$	4.37	4.62	4.57[a]	4.37	4.14	3.83

[a]Reference 54, DFT-GGA (PW91) calculations using the pseudopotential plane-wave approach.

spectively, thus the first Ir-Ir interlayer spacing expands slightly more, by 1.87% relative to the clean surface, while again the second interlayer distance is unchanged. At 0.50 ML coverage, the O atoms adsorb in "off" fcc-hollow sites, i.e., they are displaced slightly from the center of the fcc site by 0.025 Å. For the coverages 0.5, 0.75 and 1.0 ML, the first Ir interlayer spacing is expanded by about 2.74% relative to the clean surface. With regard to the O-Ir bond lengths, we find a slight decrease (of 2.07 to 2.02 Å) on going from 0.11 ML to 1.0 ML. Such a behavior of the O-Ir bond length with coverage has also been found for other O/TM systems.[11,15]

E. Electronic properties

Turning now to the electronic properties, we analyze the work-function change, $\Delta\Phi$, with oxygen coverage on Ir(111), and compare the results with O/Rh(111)[11] and O/Au(111).[83] In Fig. 4(b), it can be seen that the trend is similar to Rh(111), except that the work-function change for Rh is initially (i.e., for $0.25 \leq \Theta \leq 0.5$) steeper. At $\Theta = 0.5$ ML, the work-function change is 0.528 eV, which is in good agreement with the experimental value 0.56 eV.[84] Figure 4(b) shows the work-function change increases as a function of coverage and reaches a saturation value at $\Theta = 0.75$ ML. The reason for such an increase is the high electronegativity of oxygen inducing partial electron transfer from the substrate to the O atom, and consequently giving rise to an inward pointing surface dipole moment (with the negative charge at the vacuum side of the surface). At lower coverages, O adatoms are partially negatively charged inducing an adsorbate-adsorbate repulsion. With the increase in coverage, to reduce this repulsion, there will be partial electron transfer back to the substrate, giving rise to a decrease in the surface dipole moment, resulting in a depolarization [as shown in Fig. 4(c)]. For O/Au(111) the work-function change for 0.25 and 0.50 ML falls in between the values for O/Ir(111) and O/Rh(111), but for higher coverages (0.75 ML and 1.0 ML), the value increases much more steeply. This is in agreement with experimental result.[85]

To analyze the electron redistribution for O adsorption on Ir(111) at 0.25 ML, the difference electron density is shown in Fig. 5(a) in a plane perpendicular to the surface. The change in charge density is localized on both the first and second layers of Ir atoms and on the O atom. The valence electrons of the Ir atoms closest to the O atoms are polarized, where there is a depletion of electron density of the *d*-states oriented toward the O atom and an enhancement in the *d*-states perpendicular to these. There is also a significant depletion of more delocalized electrons in the region below the O atom, while there is an accumulation of electron density at the O atom, as well as a polarization. The Ir atoms in the second layer exhibit a redistribution of the *d*-states of opposite nature to that of the Ir atoms in the first layer, namely, an enhancement of electron density in the *d*-orbitals oriented toward the O atoms (and toward the upper O-bonded Ir atoms), and a depletion in those perpendicular to this direction. The charge transfer from the neighboring Ir atoms to the O atoms is about 0.51 according to the Mulliken

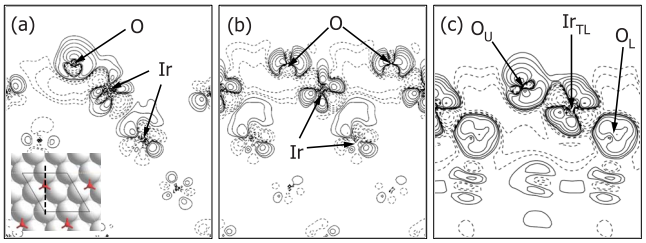

FIG. 5. (Color online) Difference electron density for (a) 0.25 ML and (b) 1.00 ML of oxygen adsorbed on Ir(111) in the fcc-hollow site and for (c) the $\sqrt{3}/(2\times2)$ trilayer structure. The contour plot depicts the $[\bar{2}11]$ plane perpendicular to the Ir(111) surface and passing through the O atoms. The inset in (a) shows, as an example, this plane in relation to the surface atomic geometry (top view) of the 0.25 ML structure. The dotted lines represent charge depletion and the solid lines represent charge accumulation. The lowest positive contour line is at 0.001 electron Bohr^{-3}, while the highest negative contour line corresponds to a value of -0.001 electron Bohr^{-3}. In between, the electron density changes successively by a factor of $10^{1/3}$ electron Bohr^{-3}.

population analysis. The difference electron density for 1.0 ML is shown in Fig. 5(b). Comparing with the 0.25 ML case [in Fig. 5(a)], it can be seen that enhancement of charge on the O atom occurs mainly in the p_{xy} states; this is due to "through" O-O interactions as the O atoms are bonded to Ir atoms, that are also bonded to other O atoms. The difference electron density for the $\sqrt{3}/(2\times2)$ trilayer structure [Fig. 5(c)] shows a significant enhancement of electron density on both the upper and lower O atoms, while it shows a strong decrease in the *d*-states oriented toward the O atoms of the Ir atoms in the center of the trilayer. On the other hand, there is a notable enhancement of the *d*-states oriented perpendicular to the O-Ir-O bond of these Ir atoms. There is little perturbation to the electron density of the Ir atoms of the underlying (111) substrate.

The nature of the O-Ir bond is characterized by a hybridization between the O-2*p* and Ir-5*d* orbitals. This can be seen from the corresponding partial density of states (PDOS) shown in Fig. 6. Considering the PDOS, it can be seen that there is a broadening and shifting of the atomic O energy levels to lower energies, and the oxygen levels are split into bonding and antibonding states. The bonding states are around 5.5–7.5 eV below the Fermi level and the antibonding states mainly around 1–2 eV above the Fermi level, where they are only partially occupied. The weight of the O-2*p* states are on the bonding states, resulting in a rather strong bond between oxygen and the Ir surface. It can be seen from the PDOS that with increase in coverage, from the 0.25 ML to 1.0 ML, occupation of the antibonding states increases slightly. This behavior is consistent with the binding energy decreasing with increase in O coverage.

IV. BULK IRIDIUM OXIDE IrO_2

It is useful to consider the properties and structure of bulk iridium oxide. There are two kinds of iridium oxide, i.e., iridium dioxide IrO_2 and diiridium trioxide Ir_2O_3. The

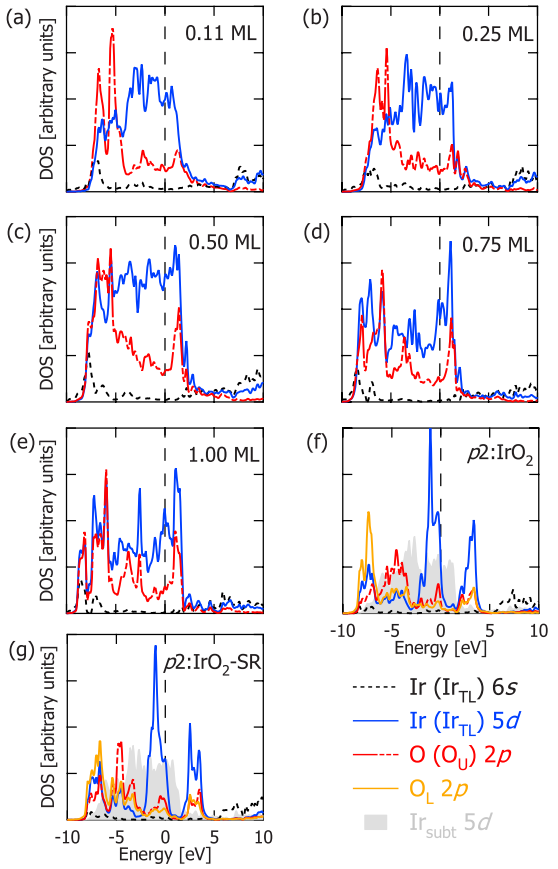

FIG. 6. (Color online) Projected density of states for the O/Ir(111) system with O in the fcc-hollow site for various coverages as indicated. Also the PDOS for the two $\sqrt{3}/(2\times2)$ trilayer structures are shown. O_U, O_L, Ir_{sub}, Ir_{TL} denote the oxygen atoms in the uppermost layer of the trilayer, the oxygen atoms in the lower layer of the trilayer, the iridium atoms in the center of the trilayer, and the iridium atoms in the first unreconstructed layer of the underlying Ir(111) substrate. The Fermi energy is indicated by the vertical dotted line at 0 eV.

former is the most common oxide of Ir and has the rutile structure, which is shown in Fig. 7.

The space group of the rutile structure is $P42/mnm$, which is nonsymmorphic. The point-group symmetries at the Ir-atom and O-atom sites are D_{2h} and C_{2v}, respectively. We summarize the calculated properties of bulk IrO_2 and compare with experiment and other DFT calculations in Table IV. In particular, we list the lattice constants, the shortest bond lengths of Ir-Ir, Ir-O and O-O, the bulk modulus, and the heat of formation. For the lattice parameter, our DFT-GGA calculation overestimates by 1% compared to experiment. The experimental value of the standard enthalpy of formation is −1.42 eV,[79] which agrees very closely with the present result of −1.45 eV.

The band structure of bulk IrO_2 is shown in Fig. 8 and the PDOS is shown in Fig. 7. It can be seen that in the energy interval around −2.0 and −1.0 eV, there is a very large peak, similar to that of the $\sqrt{3}/(2\times2)$ trilayer structure [see Fig. 6(f)].

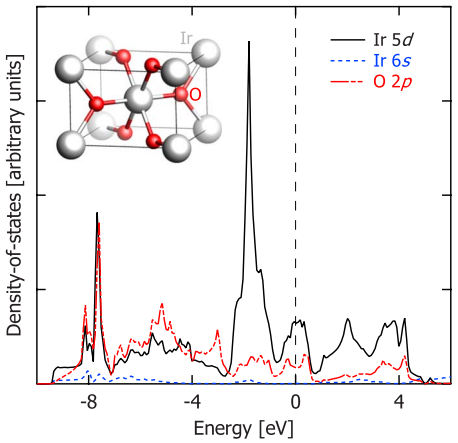

FIG. 7. (Color online) The rutile structure (inset) of IrO_2 where the small (red) spheres represent oxygen and the gray, iridium. PDOS of IrO_2 where the gray line denotes the oxygen $2p$ states and the black continuous and dashed lines iridium $5d$ and $6s$, respectively. The Fermi energy is represented by the vertical dashed line.

V. THERMODYNAMIC PHASE DIAGRAM OF THE O/Ir(111) SYSTEM

We now use Eqs. (5) and (6) to explore the effect of pressure and temperature on the stability of the various surface structures. We calculate the Gibbs free energy as a function of oxygen chemical potential and determine the relative stability range of each configuration (kinetic limitations are ignored). The result is presented in Fig. 9 where the oxygen chemical potential is correlated with pressure for three selected temperatures. Figure 10 shows the two-dimensional (p,T) phase diagram, where only the energetically most stable structures appear. From Fig. 9, it can be seen that for low chemical potentials of oxygen up to $\Delta\mu_O=-1.58$ eV, the clean Ir(111) surface is energetically most stable. Upon increasing $\Delta\mu_O$ from −1.58 eV, we find that on-surface adsorption at the fcc-hollow site with oxygen coverage of 0.25 ML starts to be energetically favored over the clean surface. Beyond $\Delta\mu_O=-1.45$ eV, the thermodynamically most stable phase is bulk iridium dioxide. From Fig. 10 it can be seen that at a pressure of about 10^{-10} atm and 700 K, bulk IrO_2 is the thermodynamically stable phase. Various experimental reports have claimed oxidation of Ir(111) occurs at around 600–800 K and at a pressure of about 10^{-10} bar ($\sim10^{-10}$ atm),[44,50–52] thus in accord with the theoretical result. Figure 10 shows clearly the three predicted stable phases of the O/Ir(111) system; the clean Ir(111) surface, the (2×2)-O/Ir(111) adsorption structure, and bulk iridium dioxide. From Fig. 9, it can furthermore be seen that if full oxidation of the surface cannot occur, e.g., due to kinetic hindering, the metastable trilayer structure becomes energetically favorable for $\mu_O\geq-0.65$ eV.

Comparing the present (p,T) phase diagram with other reported ones for O/Ag(111),[20] O/Au(111),[28] O/Pd(111),[17,18] O/Rh(111),[15] O/Ru(0001),[10] O/Pt(111),[27] and O/Cu(111),[5] we find that the O/Ir(111) system is closest to O/Rh(111) in which thin surface-oxide-like configurations are only metastable with respect to bulk oxide formation. The experimen-

TABLE IV. Calculated properties of bulk IrO_2 and comparison with experiment and other DFT calculations. Specifically, the lattice constants a and c, the nearest distance between iridium atoms $d_{\text{Ir-Ir}}$ and oxygen atoms $d_{\text{O-O}}$, and the Ir-O bond length $d_{\text{Ir-O}}$, all given in Å. The bulk modulus B_0 (in GPa) and the enthalpy of formation $H^f_{IrO_2}$ (in eV/O atom).

	Lattice const.	$d_{\text{Ir-Ir}}$	$d_{\text{O-O}}$	$d_{\text{Ir-O}}$	B_0	$H^f_{IrO_2}$
Present	$a=4.54$	3.59	2.47	1.98	253	1.45
work	$c=3.19$					
Experiment[a]	$a=4.50$	3.55	2.46	1.95		1.42[b]
	$c=3.154$					
Other *ab initio*	$a=4.51$ [c]			1.87[d]	266[e]	1.11[f]
results	$c=3.158$ [f]					

[a]Reference 86 (except the heat of formation).
[b]Reference 79.
[c]Reference 87.
[d]Reference 88, calculated using unrestricted hybrid DFT (UB3LYP).
[e]Reference 89, calculated using DFT-LDA.
[f]Reference 90.

tal observation of such metastable surface oxides for the O/Rh(111) system is due to kinetic hindering effects, which could also possibly occur for the O/Ir(111) system. Indeed, a very recent work[91] by He *et al.* studied the oxidation of Ir(111) using the technique of *in situ* surface x-ray diffraction, combined with DFT calculations. At moderately low temperatures of about 600 K and pressures of up to 100 mbar ($\sim 10^{-1}$ atm), they observe that the layered oxidic structures formed on Ir(111) which are kinetically stabilized, very similar to that of the O/Rh(111) system. Thus, this finding strengthens and supports our prediction that the $\sqrt{3}/(2\times 2)$ trilayer surface oxide structures may be observed on Ir(111) if kinetic hindering occurs. This is also in accord with the DFT calculations performed in the same study.[91] Concerning other oxygen/metal systems, first-principles (p,T) phase diagrams obtained for the O/Ag(111), O/Pd(111), and O/Au(111) systems, in contrast, predict the thermodynamic stability of thin surface oxide structures, prior to formation of the bulk oxide phase.

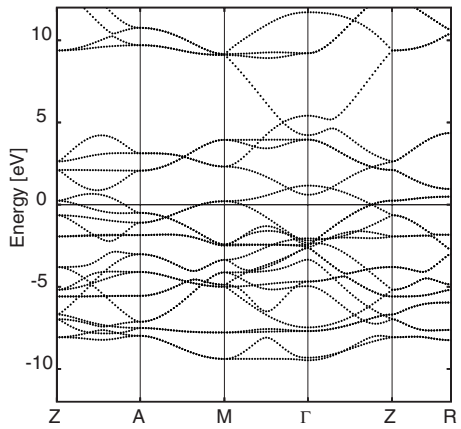

FIG. 8. Band structure of IrO_2, where the energy zero is the Fermi level.

VI. CONCLUSION

We have investigated the adsorption and interaction of atomic oxygen on the Ir(111) surface through first-principles DFT-GGA calculations. We find that for on-surface adsorption, the fcc-hollow site is energetically most favorable for all coverages considered (0.11 to 1.0 ML). In the coverage

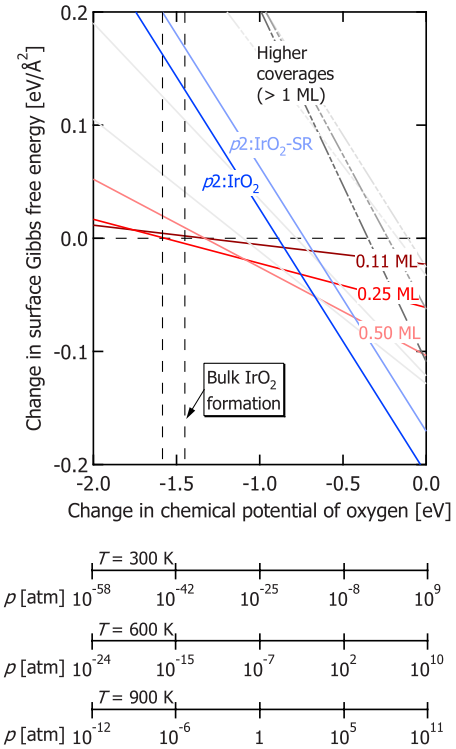

FIG. 9. (Color online) Calculated Gibbs free energy of adsorption, $\gamma(p,T)$ [cf. Eq. (5)], for the various oxygen-containing surface structures, as a function of oxygen chemical potential $\Delta\mu_O$ [cf. Eq. (6)]. The corresponding pressure scales are given for three selected temperatures [cf. Eq. (6)].

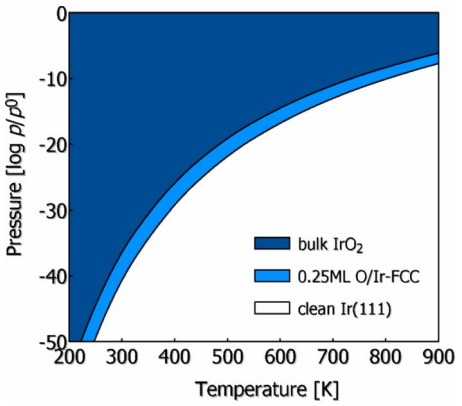

FIG. 10. (Color online) Surface (p,T) phase diagram showing the stability range of the lowest energy structures.

range 0.11 to 0.25 ML, the binding energy increases indicating an attractive interaction between the O atoms and the possible formation of a local $p(2\times2)$ periodicity.[92] With increasing oxygen coverage beyond 0.25 ML, the binding energy decreases due to a buildup of a significant repulsive interaction between the adsorbates. Pure subsurface adsorption under the first Ir(111) layer is notably less stable than on-surface adsorption and is endothermic with respect to (half) the theoretical binding energy of the O_2 molecule. For oxygen coverages greater than 1 ML, we considered mixed on-surface+subsurface structures involving a full ML of on-surface oxygen and subsurface oxygen. Incorporation of oxygen at the subsurface sites decreases the average binding energy, as compared to the on-surface chemisorption structures. However, upon increasing the subsurface oxygen concentration (from 0.5 to 1 ML), an effective attractive interaction between the O atoms is found.

We also considered the possible formation of reconstructed surface-oxide-like structures, namely the $p2:IrO_2$ and $p2:IrO_2$-SR surface structures. These O-Ir-O trilayer structures can be described as a $(\sqrt{3}\times\sqrt{3})R30°$ oxide layer on a $p(2\times2)/\mathrm{Ir}(111)$ surface unit cell, with the trilayer of the latter structure laterally shifted with respect to the former. These configurations are energetically favored for oxygen coverages greater than around 0.9 ML. To determine the predicted thermodynamically stable phases as a function of oxygen gas pressure and temperature, we used the approach of *ab initio* atomistic thermodynamics to evaluate the surface phase diagram for O/Ir(111). We find that only three different phases are predicted to be stable, namely, the clean Ir(111) surface, chemisorption of O at a coverage of 0.25 ML with a $p(2\times2)$ surface unit cell, and the bulk oxide phase. The $\sqrt{3}/(2\times2)$ trilayer surface oxide structure is predicted to form on Ir(111) only when kinetic hindering occurs. This is supported by a very recent study on the oxidation of this surface by *in situ* experimental techniques, as well as DFT.[91]

ACKNOWLEDGMENTS

We gratefully acknowledge support from the Australian Partnership for Advanced Computing National facility, the Australian Centre for Advanced Computing and Communication, and the Australian Research Council. We thank Mira Todorova for fruitful discussions.

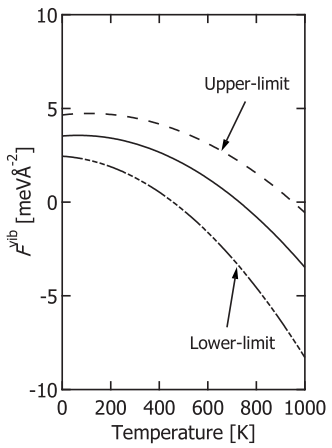

FIG. 11. An estimate of the vibrational contribution to the free energy of adsorption for O/Ir(111) [$\Theta=0.25$ ML], cf. Eq. (A1), in a temperature range of 0 to 1000 K. The vertical vibrational mode is calculated to be 60 meV (Refs. 54 and 55), while the lateral modes are estimated by varying this vertical mode by $\pm50\%$. The (middle) solid line is taken as a reference whereby all three vibrational modes are equal, i.e., without variation, while the dashed and dashed-dotted lines correspond to the upper and lower limits to the total vibrational contribution.

APPENDIX: VIBRATIONAL CONTRIBUTIONS TO THE FREE ENERGY OF ADSORPTION

The vertical vibrational mode of O on Ir(111) at an oxygen coverage of 0.25 ML has been calculated using a pseudopotential plane-wave basis set within the DFT-GGA framework.[54,55] It is found to be 483 cm^{-1}, which translates to about 60 meV. For this study, we estimate the two lateral (in-plane) vibrational modes by varying this vertical mode by $\pm50\%$, allowing us to define an upper and lower limit to the total vibrational contribution. Thus the total vibrational contribution can be written as a sum of the vibrational free-energy contribution due to the vertical mode and that due to the estimated two lateral modes.

The vibration contribution to the free energy of adsorption, F^{vib}, can be formally written as

$$F^{\mathrm{vib}}(T,\bar{\omega}) = \frac{1}{2}\hbar\bar{\omega} + k_B T \ln(1 - e^{-\hbar\bar{\omega}/k_B T}), \qquad \text{(A1)}$$

whereby $\bar{\omega}$, $\hbar$, k_B and T are the vibrational mode, the reduced Planck's constant, the Boltzmann's constant, and the temperature of the system, respectively. Using Eq. (A1) and normalizing with respect to a $p(2\times2)$ surface area, the vibrational contribution to the free energy of adsorption is plotted in Fig. 11. The (middle) solid line is drawn as a reference for the case when all three modes have the value of 60 meV. The upper and lower limits are shown as the dashed curve and

dashed-dotted curve, respectively, in Fig. 11. These plotted values are comparable to the values reported for other oxygen-metal systems and are well within ± 10 meV/Å^2 for temperatures up to 1000 K. Thus, for the present study, vibrations may be neglected without affecting the physical conclusions drawn.

*Corresponding author; aloysius@physics.usyd.edu.au

[1] C. Stampfl, Catal. Today **105**, 17 (2005).
[2] K. Reuter, C. Stampfl, and M. Scheffler, in *Handbook of Materials Modeling, Fundamental Models, Methods*, edited by Sydney Yip (Springer, Berlin, 2005), Vol. 1.
[3] C. Stampfl, M. V. Ganduglia-Pirovano, K. Reuter, and M. Scheffler, Surf. Sci. **500**, 368 (2002).
[4] H. Tang and B. L. Trout, J. Phys. Chem. B **110**, 6856 (2006).
[5] A. Soon, M. Todorova, B. Delley, and C. Stampfl, Phys. Rev. B **73**, 165424 (2006).
[6] R. Narayanan and M. A. El-Sayed, J. Phys. Chem. B **109**, 12663 (2005).
[7] G. Ertl, J. Mol. Catal. A: Chem. **182–183**, 5 (2002).
[8] F. Besenbacher and J. K. Nørskov, Prog. Surf. Sci. **44**, 5 (1993).
[9] E. Lundgren, A. Mikkelsen, J. N. Andersen, G. Kresse, M. Schmid, and P. Varga, J. Phys.: Condens. Matter **18**, R481 (2006).
[10] C. Stampfl, S. Schwegmann, H. Over, M. Scheffler, and G. Ertl, Phys. Rev. Lett. **77**, 3371 (1996).
[11] C. Stampfl and M. Scheffler, Phys. Rev. B **54**, 2868 (1996).
[12] C. Stampfl, H. J. Kreuzer, S. H. Payne, and M. Scheffler, Appl. Phys. A: Mater. Sci. Process. **69**, 471 (1999).
[13] K. Reuter, M. V. Ganduglia-Pirovano, C. Stampfl, and M. Scheffler, Phys. Rev. B **65**, 165403 (2002).
[14] K. Reuter, C. Stampfl, M. V. Ganduglia-Pirovano, and M. Scheffler, Chem. Phys. Lett. **352**, 311 (2002).
[15] M. V. Ganduglia-Pirovano, K. Reuter, and M. Scheffler, Phys. Rev. B **65**, 245426 (2002).
[16] M. Chen, S. P. Bates, R. A. van Santen, and C. M. Friend, J. Phys. Chem. B **101**, 10051 (1997).
[17] M. Todorova, K. Reuter, and M. Scheffler, Phys. Rev. B **71**, 195403 (2005).
[18] E. Lundgren, J. Gustafson, A. Mikkelsen, J. N. Andersen, A. Stierle, H. Dosch, M. Todorova, J. Rogal, K. Reuter, and M. Scheffler, Phys. Rev. Lett. **92**, 046101 (2004).
[19] D. B. Kokh, R. J. Buenker, and J. L. Whitten, Surf. Sci. **600**, 5104 (2006).
[20] W. X. Li, C. Stampfl, and M. Scheffler, Phys. Rev. Lett. **90**, 256102 (2003).
[21] A. Michaelides, M.-L. Bocquet, P. Sautet, A. Alavi, and D. A. King, Chem. Phys. Lett. **367**, 344 (2003).
[22] A. Michaelides, K. Reuter, and M. Scheffler, J. Vac. Sci. Technol. A **23**, 1487 (2005).
[23] M. Schmid, A. Reicho, A. Stierle, I. Costina, J. Klikovits, P. Kostelnik, O. Doubay, G. Kresse, J. Gustafson, E. Lundgren, J. N. Anderson, H. Dosch, and P. Varga, Phys. Rev. Lett. **96**, 146102 (2006).
[24] J. Schnadt, A. Michaelides, J. Knudsen, R. T. Vang, K. Reuter, E. Lægsgaard, M. Scheffler, and F. Besenbacher, Phys. Rev. Lett. **96**, 146101 (2006).
[25] A. Eichler, F. Mittendorfer, and J. Hafner, Phys. Rev. B **62**, 4744 (2000).
[26] D. C. Ford, Y. Xu, and M. Mavrikakis, Surf. Sci. **587**, 159 (2005).
[27] P. Légaré, Surf. Sci. **580**, 137 (2005).
[28] H. Shi and C. Stampfl, Phys. Rev. B **76**, 075327 (2007).
[29] M. Todorova, W. X. Li, M. V. Ganduglia-Pirovano, C. Stampfl, K. Reuter, and M. Scheffler, Phys. Rev. Lett. **89**, 096103 (2002).
[30] M. A. Van Hove, Catal. Today **113**, 133 (2006).
[31] A. Baraldi, S. Lizzit, G. Comelli, M. Kiskinova, R. Rosei, K. Honkala, and J. K. Nørskov, Phys. Rev. Lett. **93**, 046101 (2004).
[32] I. J. Malik and J. Hrbek, J. Phys. Chem. **95**, 10188 (1991).
[33] S. Marchini, C. Sachs, and J. Wintterlin, Surf. Sci. **592**, 58 (2005).
[34] M. K. Rose, A. Borg, J. C. Dunphy, T. Mitsui, D. F. Ogletree, and M. Salmeron, Surf. Sci. **547**, 162 (2003).
[35] B. A. Banse and B. E. Koel, Surf. Sci. **232**, 275 (1990).
[36] M. A. Mendez, W. Oed, A. Fricke, L. Hammer, K. Heinz, and K. Müller, Surf. Sci. **253**, 99 (1991).
[37] M. Pedio, L. Becker, B. Hillert, S. D'Addato, and J. Haase, Phys. Rev. B **41**, 7462 (1990).
[38] J. Haase and H. J. Kuhr, Surf. Sci. **203**, L695 (1988).
[39] B. Luo and J. Urban, J. Phys.: Condens. Matter **3**, 2873 (1991).
[40] J. F. Weaver, J.-J. Chen, and A. L. Gerrard, Surf. Sci. **592**, 83 (2005).
[41] X. Y. Deng, B. K. Min, A. Guloy, and C. M. Friend, J. Am. Chem. Soc. **127**, 9267 (2005).
[42] W. Chen, I. Ermanoski, and T. E. Madey, J. Am. Chem. Soc. **127**, 5014 (2005).
[43] S. G. Karseboom, J. E. Davis, and C. B. Mullins, Surf. Sci. **398**, 11 (1998).
[44] N. W. Cant and W. K. Hall, J. Catal. **16**, 220 (1970).
[45] D. Morales-Morales, D. W. Lee, Z. H. Wang, and C. M. Jensen, Organometallics **20**, 1144 (2001).
[46] A. Haynes, J. M. Pearson, P. W. Vickers, J. P. H. Charmant, and P. M. Maitlis, Inorg. Chim. Acta **270**, 382 (1998).
[47] C. Wögerbauer, M. Maciejewski, and A. Baiker, Appl. Catal., B **34**, 11 (2001).
[48] J. C. L. Cornish and N. R. Avery, Surf. Sci. **235**, 209 (1990).
[49] C. M. Chan and W. H. Weinberg, J. Chem. Phys. **71**, 2788 (1979).
[50] H. Conrad, J. Kuppers, F. Notschke, and A. Plagge, Surf. Sci. **69**, 668 (1977).
[51] P. A. Zhdan, G. K. Boreskov, A. I. Boronin, W. F. Egelhoff, and W. H. Weinberg, Surf. Sci. **61**, 25 (1976).
[52] T. S. Marinova and K. L. Kostov, Surf. Sci. **185**, 203 (1987).
[53] J. E. Davis, P. D. Nolan, S. G. Karseboom, and C. B. Mullins, J. Chem. Phys. **107**, 943 (1997).
[54] Y. Xu and M. Mavrikakis, J. Chem. Phys. **116**, 10846 (2002).
[55] W. P. Krekelberg, J. Greeley, and M. Mavrikakis, J. Phys. Chem. B **108**, 987 (2004).
[56] H. Over, Y. D. Kim, A. P. Seitsonen, S. Wendt, E. Lundgren, M.

Schmid, P. Varga, A. Morgante, and G. Ertl, Science **287**, 1474 (2000).
[57] B. Delley, J. Chem. Phys. **92**, 508 (1990).
[58] B. Delley, J. Chem. Phys. **113**, 7756 (2000).
[59] J. P. Perdew, K. Burke, and M. Ernzerhof, Phys. Rev. Lett. **77**, 3865 (1996).
[60] J. L. F. Da Silva, C. Stampfl, and M. Scheffer, Surf. Sci. **600**, 703 (2006).
[61] K. Reuter and M. Scheffler, Phys. Rev. B **65**, 035406 (2001).
[62] D. R. Stull and H. Prophet, *JANAF Thermochemical Tables*, 2nd ed. (U.S. National Bureau of Standards, Washington, DC, 1971).
[63] W. X. Li, C. Stampfl, and M. Scheffler, Phys. Rev. B **68**, 165412 (2003).
[64] E. Vasco, Phys. Rev. B **69**, 075412 (2004).
[65] E. D. German and M. Sheintuch, J. Phys. Chem. A **109**, 7957 (2005).
[66] C. Kittel, *Introduction to Solid State Physics* (Wiley, New York, 1986), pp. 23, 55, and 57.
[67] T. Pawluk, Y. Hirata, and L. C. Wang, J. Phys. Chem. B **109**, 20817 (2005).
[68] H. L. Skriver and N. M. Rosengaard, Phys. Rev. B **46**, 7157 (1992).
[69] H. B. Michaelson, J. Appl. Phys. **48**, 4729 (1977).
[70] C. M. Chan, S. L. Cunningham, M. A. Van Hove, W. H. Weinberg, and S. P. Withrow, Surf. Sci. **66**, 394 (1977).
[71] M. V. Ganduglia-Pirovano and M. Scheffler, Phys. Rev. B **59**, 15533 (1999).
[72] S. Schwegmann, H. Over, V. De Renzi, and G. Ertl, Surf. Sci. **375**, 91 (1997).
[73] D. L. Adams, H. B. Nielsen, and M. A. Van Hove, Phys. Rev. B **20**, 4789 (1979).
[74] M. Kaack and D. Fick, Surf. Sci. **342**, 111 (1995).
[75] Y. Xu and M. Mavrikakis, Surf. Sci. **494**, 131 (2001).
[76] W. X. Li, C. Stampfl, and M. Scheffler, Phys. Rev. B **65**, 075407 (2002).
[77] K. Huber and G. Herzberg, *Molecular Spectra and Molecular Structure IV: Constants of Diatomic Molecules* (Van Nostrand Reinhold, New York, 1979).
[78] J. Gustafson, A. Mikkelsen, M. Borg, E. Lundgren, L. Köhler, G. Kresse, M. Schmid, P. Varga, J. Yuhara, X. Torrelles, C. Quirós, and J. N. Andersen, Phys. Rev. Lett. **92**, 126102 (2004).
[79] D. R. Lide, *CRC Handbook of Chemistry and Physics, Internet Version 2005* (CRC, Boca Raton, FL, 2005).
[80] K. Tanaka and K. Tamaru, J. Catal. **2**, 366 (1963).
[81] B. Hammer and J. K. Nørskov, Adv. Catal. **45**, 71 (2001).
[82] G. V. Samsonov, *The Oxide Handbook* (IFI/Plenum, New York, 1973).
[83] H. Shi, R. Asahi, and C. Stampfl, Phys. Rev. B **75**, 205125 (2007).
[84] V. P. Ivanov, G. K. Boreskov, V. I. Savchenko, W. F. Egelhoff, Jr., and W. H. Weinberg, Surf. Sci. **61**, 207 (1976).
[85] N. Saliba, D. H. Parker and B. E. Koel, Surf. Sci. **410**, 270 (1998).
[86] A. A. Bolzan, C. Fong, B. J. Kennedy, and C. Howard, Acta Crystallogr., Sect. B: Struct. Sci. **53**, 373 (1997).
[87] S. H. Brewer, D. Wicaksana, J. Maria, A. Kingon, and S. Franzen, Chem. Phys. **313**, 25 (2005).
[88] M. Okumura, Y. Irie, Y. Kitagawa, T. Fujitani, Y. Maeda, T. Kasai, and K. Yamaguchi, Catal. Today **111**, 311 (2006).
[89] H. W. Hugosson, G. E. Grechnev, R. Ahuja, U. Helmersson, L. Sa, and O. Eriksson, Phys. Rev. B **66**, 174111 (2002).
[90] T. H. Siddall and C. A. Prohaska, Nature (London) **208**, 582 (1965); T. H. Siddall, Tetrahedron Lett. **6**, 4515 (1965).
[91] Y. B. He, A. Stierle, W. X. Li, A. Farkas, N. Kasper, and H. Over, J. Phys. Chem. C (to be published).
[92] H. Tang, A. Van der Ven, and B. L. Trout, Phys. Rev. B **70**, 045420 (2004).